applied optics

Tear film imager for dynamic mapping of the human tear film

Yoel Cohen,[1] Shlomi Epshtein,[1] Alon Harris,[2] Raanan Gefen,[1] Lawrence Kagemann,[3,4,5] and Yoel Arieli[6,*]

[1]AdOM Advanced Optical Methods, Hamlacha 1, Lod, 7152001, Israel
[2]Indiana University, School of Medicine, Glick Eye Institute 1160 W. Michigan St., Indianapolis, Indiana 46202, USA
[3]U.S. Food and Drug Administration, Silver Spring, Maryland 20993, USA
[4]New York University School of Medicine, New York, New York 10016, USA
[5]Department of Ophthalmology, School of Medicine, University of Maryland, Baltimore, Maryland 21201, USA
[6]Jerusalem College of Technology, Jerusalem 9372115, Israel
*Corresponding author: arieli.yoel@gmail.co

Received 18 February 2019; revised 17 June 2019; accepted 7 August 2019; posted 7 August 2019 (Doc. ID 360423); published 4 October 2019

Dry eye (DE) disease is a multifactorial disease of the outer ocular surface characterized by several ocular symptoms and mainly by tear film instability. We have developed an optical imaging system, the tear film imager (TFI), which is the first instrument that can directly image the muco-aqueous tear layer physical dimension *in vivo* and evaluate its parameters in a noninvasive mode with nanometer axial resolution. This instrument provides quantified information about many attributes of the tear film, including muco-aqueous layer thickness, lipid layer thickness, thickness change rate, and the break-up time. The TFI performances are based on simultaneous acquisition of large field of view (FOV) imagery and fast spectrometric measurement of the interference from the thin tear film sublayers. Herein, after describing the instrument and the methodology of the measurements, we use a tear film mock-up to quantify device accuracy (2.2 nm) and repeatability (0.25 nm standard deviation). In conclusion, we present a new technology for the assessment of the tear film with an unprecedented axial resolution and excellent accuracy and reproducibility.

https://doi.org/10.1364/AO.58.007987

1. INTRODUCTION

The definition and classification subcommittee of the tear film and ocular surface international dry eye (DE) workshops (TFOS DEWS I-II) defines DE disease as "a multifactorial disease of the ocular surface characterized by a loss of homeostasis of the tear film, and accompanied by ocular symptoms, in which tear film instability and hyperosmolarity, ocular surface inflammation and damage, and neurosensory abnormalities play etiological roles" [1]. Accordingly, accurate information on the human eye tear film and its layers—the lipid layer, the aqueous layer, the mucus layer, as well as the epithelium substrate—is an important key for the understanding of DE disease status.

There are several clinical tests to assess DE. The common Schirmer test assesses outflow through the lacrimal gland by wetting the eye for 5 min with strips applied directly to the eye. It is invasive and it fails to describe the tear film. The osmolarity test by TearLab [2] measures the tear film's solute concentration. It is an invasive test, limited by large variance, resulting in the need to repeat the test three times in each eye. The result provides just one parameter for DE health. The MMP-9 concentration test by RPS [3] is considered to be a reliable marker for inflammation. It is commonly associated with DE, but it only indicates the presence of severe cases of DE disease. Tear break-up time (TBUT) provides a quantitative parameter of the stability of the tear film. The TBUT is measured by applying fluorescein to the tear film and measuring the time until a dry spot appears, or, alternatively, by a noninvasive method that analyzes the projection of Placido's disk utilizing image processing [4]. The Lipiview device, by Johnson and Johnson, uses LED illumination to produce white light interference. It measures the color of the tear reflections and provides a parameter that represents the average lipid layer thickness on the inferior half of the cornea per measurement. Then it calculates the average over the entire measurement time [5,6]. The currently available tear film assessment technologies produce results that are difficult to interpret, specifically, parameters that are only surrogate for some aspect of tear film dynamics and show little correlation with DE symptoms [7]. Thus, a comprehensive noninvasive description of the dynamic tear film in human eyes is still in need.

The most promising noninvasive method for accurate measurement of the individual tear sublayers is interferometry [8].

The physical interference signal is recognized and verified to originate from the human tear's sublayers: the aqueous and lipid [9–11]. Such measurement can be performed both on bare eyes and on eyes wearing contact lenses. Currently, most of the noninvasive interferometry methods are still in the incubation level and have been accomplished only in laboratories for a small sample of patients. Existing commercial interferometry-based instruments, such as optical coherence tomography (OCT), suffer from limited accuracy (a few micrometers). Moreover, the main drawback of currently available instruments is that they try to measure only static parameters of the tear film sublayers. In many cases, the problems of a DE come from the instability of the tear [8,11] rather than merely the tear's layer's thicknesses.

The dynamic behavior of the tear film, even for short time intervals, is determined by multiple factors: the blinking that resets the tear structure every few seconds, the movements of the liquids following each blink and their redistributions in each sublayer, the evaporation and drainage that reduce the tear volume, and the reflex tearing that increases the muco-aqueous volume. Assessment of this dynamic system may be hindered by saccadic eye movements that change the eye orientation as well as by local tear disturbances such as bubbles and detached tissues (e.g., epithelium) that may affect the reflected image. Furthermore, the major part of the tear film layer is the muco-aqueous [1] sublayer that is characterized by low reflectance and high dynamics.

These properties pose a technological challenge, and current clinical devices struggle to extract meaningful clinical data on the muco-aqueous layer's status in specific and the tear film dynamics in general.

An interesting attempt to address the dynamic behavior of the tear was described lately, utilizing a spectral domain OCT [12]. That work demonstrated time-resolved tear film thickness measurements in the range of 2–5.5 μm with a resolution of 2.1 μm. Such technology, with improved measurement time from the currently typical 1.5 s to a fraction of a second, may be useful for patients that have sufficient aqueous layer thickness (nonaqueous-deficient). A limitation of this method is the inability to resolve the tear films' sublayers. Recently, Hwang *et al.* [13] used the Lipiscanner 1.0 system to analyze the color interference in order to deduce the lipid layer thickness. They demonstrated the use of scatter plots for the theoretical RGB color in comparison to RGB pixels distribution to correct for errors. In such mode, only the dynamics of the lipid layer could be achieved.

A noninvasive device that can provide dynamic measurements of the tear sublayers is needed. Such a DE diagnostic device should repeatedly measure the tear sublayers at a high rate to extract the sublayers' dynamics while operating in a robust mode fitting everyday implementation in the clinic.

In this paper we describe a new instrument, the Tear Film Imager (TFI), which can continuously measure the tear film sublayers' quasi-static and dynamics parameters and clinically document nonuniformities in a large field of view (FOV). The TFI automatically measures the tear sublayers' thicknesses and calculates these parameters and their trends over a time range of several blinks. This report describes the TFI principles of operation as well as measurements on a tear film mock-up verifying the TFI measurement accuracies and *in vivo* proof of concept on some eyes, validating that the TFI can assess live human eyes without intervention.

2. PRINCIPLES OF OPERATION

The TFI system has three modes of operation: color analysis of broadband light reflectance from an ultra-thin layer, spectral model-based interpretation of the interference of broadband light in a very low-contrast thin layer reflectance, and full-field imaging over a large FOV.

The lipid sublayer is characterized by an ultra-thin structure, typically 0–120 nm in thickness, lower than the wavelength of visible light. Because the layer is thinner than a single wavelength, the interference pattern of the reflectance from the top and bottom interfaces does not present constructive and destructive peaks. There is, however, a color change in the reflected light as a function of the thickness and orientation. As a result, observing the lipid layer color under broadband illumination enables the observation of the color shift and calculation of the lipid layer's thickness. Consequently, the accuracy of the lipid layer thickness measurement depends on the accuracy of the color measurement.

The muco-aqueous sublayer is characterized by a very low reflectance due to the small difference in the refractive index between its lower boundary and the surface below. This layer is much thicker than the lipid layer and can reach several micrometers (several visible wavelengths), and thus shallow destructive and constructive interference patterns may appear.

Measuring the spectral reflectance of the tear film over a large waveband and analyzing it based on an electromagnetic simulation tool enables us to distinguish between each sublayer and to calculate an accurate thickness.

Large-FOV imaging enables us to efficiently identify and mitigate sources of error such as blinks, tear flow, and eye motions. These events obstruct the regular collection of spectral data and are removed. The large FOV also allows observation of local break-up events during the measurement time.

A. System Challenges

Inhomogeneities of the tear film layers impede spectral measurements. Signals that are created by the interference from nearby areas may differ in terms of relative phase interference. This and other inhomogeneities require limiting the spectrometric sampling area and in turn may reduce the signal-to-noise ratio, which is already marginal. Applying longer integration times, which can be a solution, is limited due to tear film dynamics and eye movements. Longer integration times increase the likelihood of motion artifacts, and the interference measurements may be blurred.

On the curved cornea, large-FOV imaging requires broad angle illumination. The signal-to-noise limitation is even more pronounced in large-FOV illumination; safety considerations limit the maximal exposure of the eye. Therefore, increasing the illuminated area reduces the illumination density at each point. Previous studies [9,11] performed spectral measurements on reflected light that was collected from small illumination areas only. Performing spectral measurements on

light reflected from a large FOV may result in low signal as a result of illumination limitations and an averaging effect due to the layers' non-homogeneity. Therefore, careful optimization of the measured sampled area mitigates this effect.

Another challenge comes from the curvature of the eye. Angular movements, even small deviations in the longitudinal Z dimension or the lateral X or Y dimensions, can severely affect the measurement accuracy. As a result, when the position of the eye is not stable, the inaccuracy in the absolute measurement of the eye reflectance may lead to instability in the layer thickness interpretation [11]. Accordingly, special methods and mechanisms are required to minimize lateral deviations, to identify them promptly, and to either correct or halt the spectral measurement.

3. TFI OPTICAL SYSTEM

In order to address the aforementioned challenges, we have built an optical system, the TFI; its opto-mechanical scheme is shown in Fig. 1 [14].

The optical system has two modules: the illumination module and the imaging module. The illumination module consists of a 55 W halogen lamp as a light source. The light is focused by a condenser into an aperture of 4 mm diameter. The light transmitted by the aperture has a very large angle of divergence and is collimated by a Fresnel lens L_1 (focal length $f_1 = 130$ mm; diameter $D_1 = 140$ mm). At the end of the illumination module, the collimated light is converged towards the internal cornea with a very large solid angle of ~60° by a second Fresnel lens L_2 ($f_2 = 45$ mm; $D_2 = 140$ mm).

While L_2 directs the off-axis illumination, the objective lens L_3 ($f_3 = 45$ mm; $D_3 = 18$ mm), embedded in L_2's center, directs the on-axis illumination. The edges of the two illumination module components, L_2 and L_3, create a circular shadow on the cornea. This circular shadow, which is imaged as a dark ring on the cornea's image, is utilized for estimating the decentering of the eye's image in each acquired frame relative to the optical axis.

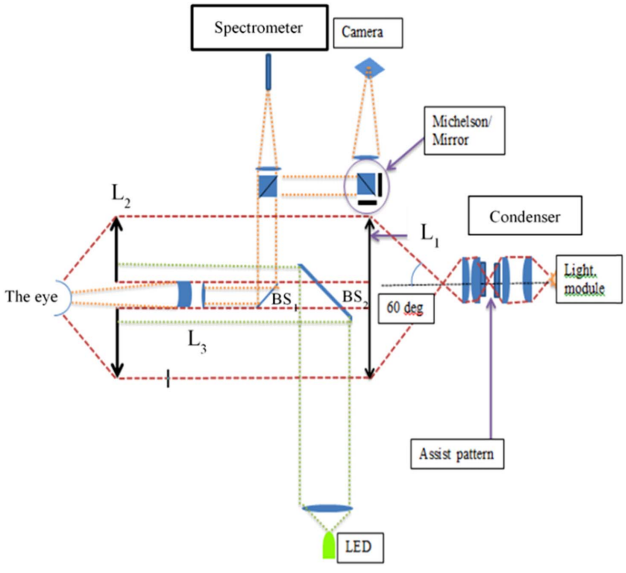

Fig. 1. Optical system of the TFI device.

The intensity of the halogen lamp illumination on the cornea is 7 mw/cm^2 with a broad angle and a broad wavelength range of 450–1150 nm. This light is further adjusted to ensure that the retinal irradiance is well below the maximum permissible exposure level for continuous measurement for both photochemical and thermal effects. The impact of the beam warming of the cornea was calculated to be less than 0.4°C during the maximum 40 s measurement period, such that it barely modifies the evaporation rate and is well below the safety limit.

The light reflected from the eye is gathered by the imaging module and is directed to a camera and a spectrometer via the objective lens L_3 and a beam splitter BS_1. After, the light is split between two imaging channels, constructing two parallel conjugate planes: one for camera imaging and one for spectral measurement. Boresight alignment between the camera center, the spectrometer measurement spot, and the imaging channel optical axis, including the object, is essential.

The spectrometric measurements use a conjugate plane to the cornea surface located at the spectrometer fiber entrance. On this plane, spectral spot measurements are sampled at a typical diameter of 250–300 μm. The spectrometer is an Ocean MayaPro 2000 grating spectrometer with 300 grooves per mm and a spectral range of 450–1150 nm operated by our custom software with a typical measurement rate of 15 times per seconds. The camera is a 2M pixel CMOS-based camera, UI-3250ML-C-HQ, produced by IDS with a grabbing rate of 10–15 frames per second. The equivalent pixel size on the cornea surface is 6 × 6 μm.

For focus estimation, assist patterns printed on a transparent plate are projected onto the cornea. This plate is positioned in a plane conjugate to the plane of the cornea in the condenser, and thus the projected patterns are also imaged by the imaging module while measuring the tear film reflections. The image of the patterns is continuously analyzed for estimating the momentary Z-axis position of the cornea relative to the optical system. The Z-axial position of the Fresnel lens L_2 and the objective L_3 is adjusted by a motor under closed-loop control, proportional to the Z-axis position analysis. The auto-focus algorithm has a fast response and fast convergence, and it corrects defocus with a tolerance of 100 μm. In the case of momentary misalignment or decentering, the acquired data is marked accordingly.

As a fixation target, a green LED introduced through a second beam splitter BS_2, allowing only 0.01 mW of the LED light to be directed into the eye. This intensity is enough to ensure that the measured eye can stare at the optical axis orientation without disturbing the measurement process or breaching the safety limits.

In order to enable interferometric measurement on top of the reflectometric measurement in the same instrument, an optional interferometric module may be added. This interferometric module can be added by inserting a third beam splitter and a Michelson interferometer in front of the camera. The interferometric module can serve as a variable spectral modulator for the broadband light of the halogen lamp by

moving one of the interferometer's mirrors by a step motor and varying the optical path difference (OPD) between the mirrors continuously while grabbing the cornea's images. By spectrally modulating the light and analyzing the intensity function of each pixel in the grabbed images, a full-field spectral measurement can be attained [15]. However, using the interferometer for full-field spectral measurements is time consuming and does not allow frequent enough sublayer dynamics measurements. The sublayers' dynamics are better deduced from the combination of the camera and the spectrometer measurements only.

4. MEASUREMENTS AND ANALYSIS

A. Spectral Measurement Interpretation

The lipid, aqueous, mucus, and the epithelium substrate roughness thicknesses are calculated based on the spectral data measured by the spectrometer. The measured spectrum is analyzed by comparing it to a simulated spectral reflectance using a rigorous model of the tear film and adjusting the model to minimize the spectral differences. The model of the tear film we use is a stacked layer including all the tear's sublayers: the lipid, aqueous, mucus, and the epithelium substrate roughness. To reach the simulated spectral reflectance closest to the real spectral reflectance values, rigorous coupled wave analysis (RCWA) [16] simulation is utilized where the lipid, aqueous, and mucus layers are represented as transparent layers and the epithelium substrate roughness is represented as a semi-periodic conic structure in the stack.

Realizing a high level of confidence for the converging RCWA simulation involves setting typical values of the tear film layers as a starting point. As nominal starting values, we have used a tear film model with lipid, aqueous, mucus, and epithelium roughness thicknesses of 34, 2000, 500, and 2000 nm, respectively. The full range of dispersion values were used, including refractive indexes and extinction coefficients, out of which the refractive values at 633 nm are: lipid layer (1.47495), aqueous layer (1.33001), mucus layer (1.36311), and struma/epithelium substrate (1.41011). The extinction coefficients were all set to zero for the full range. The starting point for aqueous layer dispersion was in accordance with Bashkatov *et al.* [17]. The dispersion values were transferred to polynomial form and were then optimized based on a group of spectra. It was found that the impact of optimization was small and negligible, and this confirmed our starting point.

Typical results of such simulation of the spectral reflectance are shown in Fig. 2, where two different stacks of equal weighted areas were simulated; one has an aqueous thickness of 2000 nm (blue curve), and the other has an aqueous thickness of 1830 nm (red curve). In both stacks, the lipid, mucus, and the epithelium substrate thicknesses roughness remained at nominal values.

The spectral reflectance oscillates as a function of the wavelength where the combined muco-aqueous thickness determines the phase of the oscillation but does not affect the reflectance average trend significantly. Another observation from Fig. 2 is that mixing the two signals (red and green) yields a spectral reflectance without oscillations (green) for the range of 800–1040 nm, which is applicable for measurement with a poor lateral resolution that integrates over an area of varying

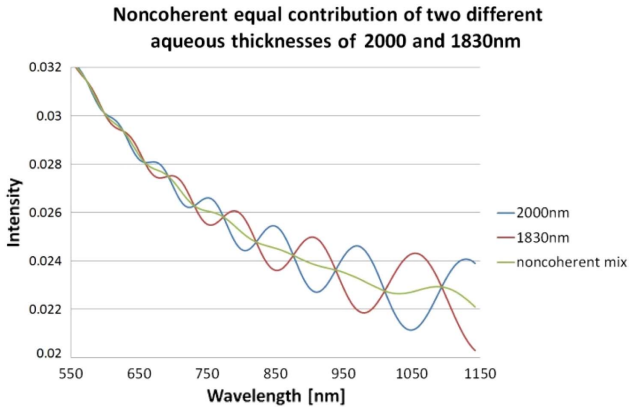

Fig. 2. Simulation of the impact of noncoherent interference of equal weight of areas that represent two different stacks: blue curve with an aqueous value of 2000 nm and red curve with an aqueous value of 1830 nm. A noncoherent equal mix of these two yields a spectrum without oscillations for the range of 800–1040 nm (green curve).

thickness, which might eliminate the aqueous oscillation signal. During the interblink interval, mainly right after the blink, high local spatial gradients appear in the tear sublayer thickness. In this case, a nonuniform thickness may exist and mixed state reflectance can appear, even at moderate spot size. A special test based on an extraction of the amplitude per wavelength information was added to the algorithmic procedure to identify uneven disturbances to the oscillation frequency and mark them as a mixed state. In case of an anomaly, such data were filtered to avoid incorrect interpretation.

These calculated spectral reflectance results served as the basis for further study of the effect of the different parameters that are involved in the tear film model on the tear film's reflectance. For each sublayer of the tear film, theoretical calculations around its nominal value were carried out: each layer's thickness was changed in small steps, while all other layers were kept at their nominal values. Investigating the sensitivity of the spectral reflectance of the tear film to the different parameters was beneficial to understanding which parameters to focus on and to target the design of a recurring algorithm with fast convergence for calculating the tear film's layers' thicknesses more rapidly.

Figure 3 shows an example of such a study, where the spectral reflectance of the tear film's layers was simulated for different stepping thicknesses values. The nominal fixed values of the lipids, mucus, and roughness of the epithelium substrate were 30, 1000, and 2000 nm, respectively, where the aqueous thickness was changed in steps of 25 nm from 1000 to 1200 nm. This figure demonstrates the sensitivity of the RCWA modeling and its ability to differentiate nanometer-scale changes in the aqueous thickness.

Figure 4 shows typical simulation results of the spectral reflectance of the tear film as a function of the lipid layer thicknesses. The nominal values of the aqueous, mucus, and the roughness of the epithelium substrate were 1000, 1000, and 3000 nm, respectively, where the lipid thickness was changed in steps of 10 nm from 0 to 120 nm. In our investigation results, the lipid layer was the most dominant

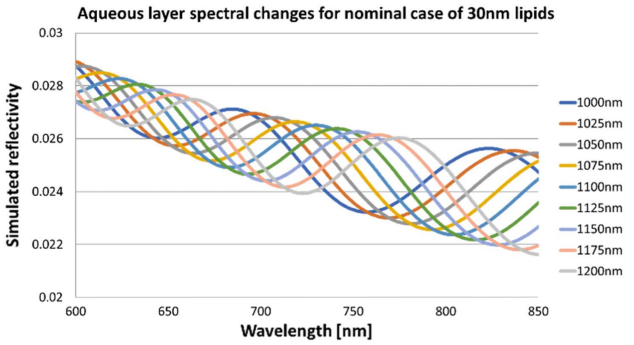

Fig. 3. Study of the sensitivity of the aqueous layer thickness by simulation of RCWA. The aqueous thickness was changed in steps of 25 nm from 1000 to 1200 nm. The other layers were kept at nominal values of 30 nm for the lipid, 1000 nm mucus, and 2000 nm for the roughness of the epithelium. A sub-range of wavelengths is presented to highlight the oscillation behavior at the best system SNR range.

layer that impacts the reflectance and its trend along the spectrum. The ability of this method to distinguish nanometer-scale changes in the lipid layer thickness is apparent from this figure.

We used similar methods to investigate the mucus and the aqueous layers' thicknesses interdependencies and have found that these two layers cannot be distinguished optically one from the other due to the gradual interface between both layers. The gradual change in the refractive index generates a very low reflectance, and the overall phase shift can be considered as a phase shift produced by only one effective medium. Such evidence for the gradual interface and the continuity of the muco-aqueous layer was also mentioned in the literature [1]. In Refs. [8–11], the muco-aqueous interface contribution to the reflectance was neglected, and simplified mathematical formalism was used. In the current work, despite the special emphasis on very weak reflectance in the physical reflectance model we use (as shown in Figs. 3 and 4), we could not observe

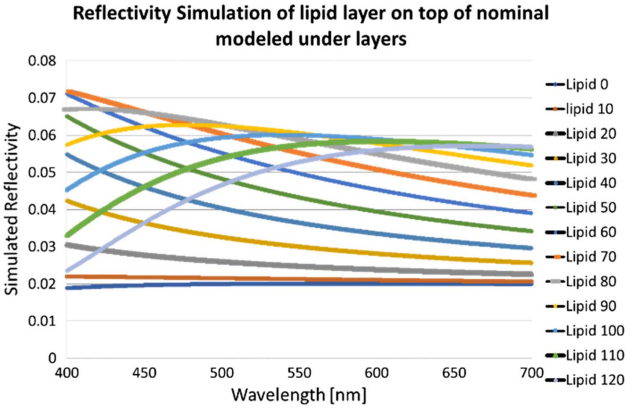

Fig. 4. Study of the sensitivity of the lipid layer thickness by RCWA simulation. The nominal value of the aqueous was 1000 nm, of the mucus was 1000 nm, and of the roughness of the epithelium substrate was 3000 nm. The lipid layer thickness was changed in steps of 10 nm from 0 to 120 nm. One can assess RGB camera's ability to distinguish lipid layer thickness changes from this figure, as the wavelength range complies with the RGB range.

the mucous and aqueous layers' interface. Accordingly, and in line with DEWS II conclusions [1], we have considered these two layers as a single layer with equivalent thickness value and named it the muco-aqueous layer.

A fast converging algorithmic methodology for calculating the tear film's layers thicknesses is used. The first step for calculating the actual tear film's layers' thicknesses performs a pre-analysis for calculating roughly the lipid's thickness based on the spectrometer measurement. Then, using the calculated thickness lipid value together with additional layers' thicknesses and epithelium roughness, a global search algorithm is performed in order to achieve the best fit to the spectrometer measurement. The calculations are ended after achieving a convergence of a 0.01 nm step-to-step improvement or after a predetermined runtime. The algorithm typically converged within several seconds per each measured spectrum. This interpretation model was found sufficient to analyze the tear film's inner structure as described below, without additional mathematical formalism or empirical value approximations as was done in previous works [9,10].

Special care was given to avoid ambiguity in the interpretation. There are two contributions that helped to overcome the ambiguity challenge: 1) the large wavelength range and 2) the dispersion of the refractive index over this range. Because the sinusoidal nature enforces similar periodicity for any order in k space, a large range of k can distinguish between the oscillation frequencies as long as this frequency has more than one cycle in the k-space range. The system wavelength range was extended to 450–1150 nm in order to ensure that more than one cycle exists down to the lower thickness values of 1500 nm muco-aqueous thickness.

Working with reliable data is a key requirement for the system setup. Image analysis algorithms for displacement and focus were used in order to filter out measurements where the data collection was outside the allowed predefined limits. The definition of those limits was based on an investigation of the impact of displacement and defocus on the reflectance values. Maximal tolerance of $\pm 0.25\%$ for absolute reflectance was implemented, which is equivalent to a tolerance of 1 and 1.4 nm for the lipid and the muco-aqueous layers' thicknesses, respectively.

The TFI was tested by measuring several eyes using the described model and algorithm as described below. So far, the results show a very good fit, suggesting that the model and the method are valid.

B. Color Camera Measurements

The color camera (RGB) provides large-FOV coverage with lower spectral resolution. One of the primary uses of the camera is monitoring the eye behavior (blinking, saccadic motion, etc.) and supporting the focus mechanism as explained previously.

In addition, based on the camera color images, the TFI can provide an assessment of the lipid layer thickness for each pixel in the FOV.

The importance of accurate spectral measurements for lipid thicknesses calculation was discussed above. However, color camera measurements tend to contain absolute intensity errors, especially under low light levels. This is emphasized in recording tilted or moving objects. Consequently, the accuracy

of this mode of calculated lipid layer thickness is in the range of 10–30 nm, which in many cases is the full range of the lipid layer thickness, i.e., ±100%. Thus, better color calibration of the camera is key for accurate full-field lipid layer thickness assessment.

To improve the camera spectral response accuracy, a dynamic calibration process for the entire FOV was developed. This process consists of a full-field calibration stage followed by a recurring dynamic color map anchoring.

The full-field calibration is based on calibrating the camera using a calibration target of a curved object imitating the eye ($D = 12.5$ mm; $f = 15$ mm Thorlabs plano-convex uncoated lens), which has a known reflectance at each color band of the camera. The images of the calibration target acquired by the camera indicate the reflected light coefficients at each color band of the camera as measured at each pixel. The measured reflected light intensities and the known reflectance of each point of the calibration target are used to calculate the color intensity transfer function of the optical system at each pixel relative to the central spot.

The calibration target image could give feedback indicating the RGB matching level per pixels in a merit form. This process could indicate areas with bad fit or offset of the camera's internal calibration. Some optional polynomial corrections can be employed, while the offset can be aided by the spectrometer measurement in the center spot. It was found that simple offset correction alone gave a correction level that improves the merit by about 90% compared with the polynomial options. For the sake of simplicity and stability, the offset simple correction was chosen to improve the recurring calibration aided by the accurate center spot spectrometric measurement.

In the following recurring color map anchoring process, the camera-measured intensities are calibrated to absolute values by using the spectrometer reflectance readings. The RGB intensities of the image's central spot are compared to the spectrometric interpreted measurements of the same spot at the matching color bands. The central spot correction ratio is applied to the other mapping pixels to correct and improve the accuracy of all pixels in the FOV. The anchoring process is repeated for every processed image.

After applying the calibrations, we assume that the difference in reflectance between different points on a certain tear film image is predominantly caused by variations in the lipid layer thickness. Consequently, a simplified lipid thickness calculation algorithm can be utilized. The algorithm is applied to each pixel in the image separately after color calibration. The calibrated measured RGB intensities are compared to predicted intensities at the same color bands that are obtained from simulated spectra of varying lipid layer thicknesses and constant muco-aqueous layer thickness equal to the thickness previously calculated on the central spot. Each pixel's lipid thickness is defined as the thickness that provided the best match between the measured and predicted RGB intensities.

A typical full-field lipid thickness map for certain muco-aqueous layers' thicknesses is shown in Fig. 5 for normal eyes. The map uses color coding for lipid values with 5 nm steps in a range of 0–130 nm. These values were calculated for each pixel using a transfer function calibration. The best lipid layer thickness match to the measured camera color intensities is presented for each pixel, and the pixel combination forms the lipid layer thickness map.

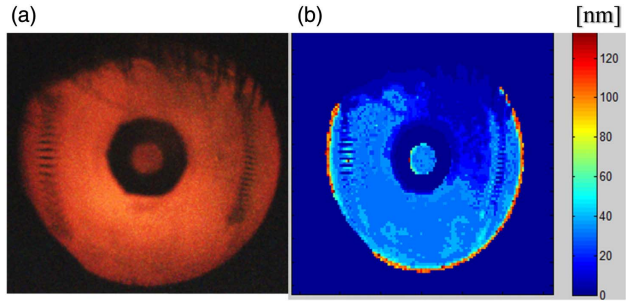

Fig. 5. Typical full-field lipid thickness map where (a) the raw image is captured by the camera, (b) the lipid thickness map is deduced from the camera color image at each pixel, after the full-field calibration and color map anchoring processes.

The raw image captured by the camera is shown in Fig. 5(a), and the thickness map that was deduced from its color information at each pixel is shown in Fig. 5(b) as a false color map. The ring in the center and the grids on both sides of the image are the shadow of the illumination channel and the assist patterns for the focusing as described above, and they are excluded from the tear film image interpretation. The color code legend on the right side of the thickness map presents the thickness values in nanometers. This color map represents the thickness values of the lipid layer with a lateral resolution of $6 \times 6\ \mu m^2$ on the cornea and thickness accuracy of ±2.5 nm. One can appreciate the high sensitivity to small thickness variations in this figure.

This normal eye lipid thickness map presents a uniform layer with delicate thickness changes. The TFI sophisticated color interpretation and anchoring that provide accurate assessment of the lipid layer thickness for each pixel is a mandatory method to evaluate such uniform layer and distinguish it from coarser ones.

Figure 6 presents the lipid thickness map as a function of the anchoring constrained value at the central spot of the image from 15 to 75 nm (same color code legend as in Fig. 5). Each of these values may be relevant, but only the value of 45 nm is the correct one according to the spectrometer measurements at the central spot. As this figure presents, non-accurate anchoring may produce thickness artifacts (pointed to by the arrows) in the image interpretation. Furthermore, insufficient calibration can result in a too-thin or too-thick assessment of the lipid layer, which in turn may lead to a wrong conclusion on the patient's lipid layer status.

The good visualization of the tear film over a large FOV as provide by the TFI enables us to monitor the tear dynamic behavior and extract the tear break-up time parameter. Tear break-up time is considered the main parameter for the tear film's dynamic stability.

5. EXPERIMENT AND RESULTS

To evaluate the performance of the TFI measurements and its interpretation algorithms, experimental measurements were

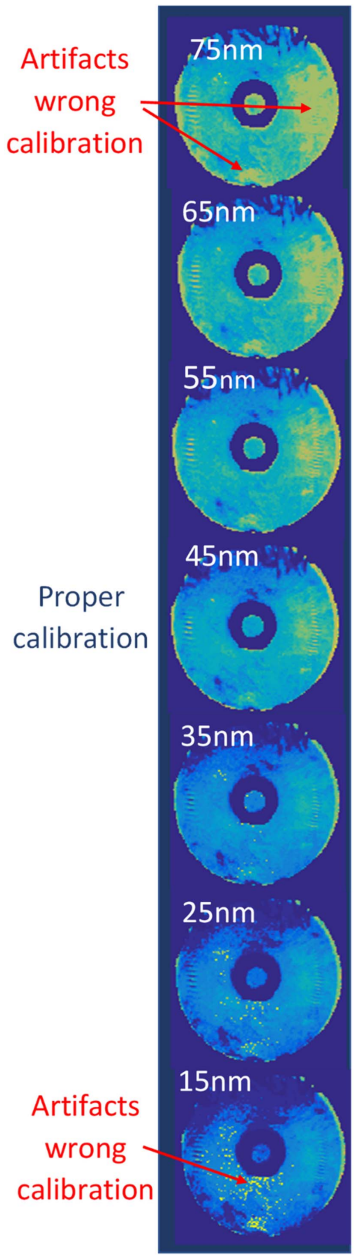

Fig. 6. Impact of the central spot thickness calibration on the camera's full-field lipid layer thickness interpretation. The values of the central spot calibration were altered from 15 to 75 nm, while only the value of 45 nm is the true one. The Fig. 5 color code for lipid layer thickness is applicable here as well.

performed on a mock-up sample imitating the ocular surface, including the tear film sublayers. The sample is a curved object made of glass N-BK7 with coatings of 60 m thin transparent silicon oxide layer on top of a 1000 nm layer of magnesium fluoride. The materials were selected to achieve similar refractive index interface differences as assumed between the tear sublayers. The coatings' thicknesses were verified by accurate ellipsometric measurements.

The TFI experiments were performed by using full repeating cycles of automatic focusing, measurement, and thickness interpretation as performed for the tear film measurement.

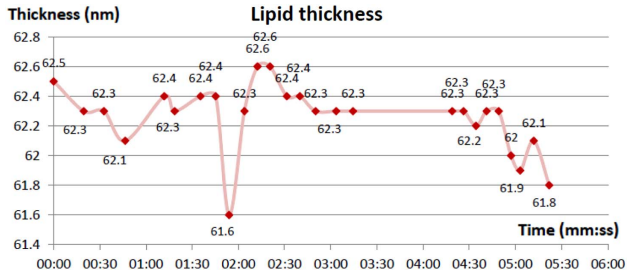

Fig. 7. Repeatability measurements of the lipid layer mock-up (while measuring the tear film mock-up) over 5.5 min.

In these experiments, the accuracy was found to be 2.2 nm and repeatability was 0.25 nm (standard deviation) for both the upper and the lower layers. An example of the repeatability measurements for a 5.5 min period is shown in Fig. 7.

The TFI was also tested by measuring human eyes during a clinical study (Helsinki 0166-13-MMC) [18]. This TFI pilot clinical study at Meir Medical Center, Israel, proves the repeatability of its muco-aqueous measurements and the ability to differentiate between different states of DE disease [19]. The study involved 49 patients with a mean age of 58.8 years. Reproducibility of the muco-aqueous tear layer thickness was excellent ($r = 0.88$) and significantly correlated with the Schirmer score ($r = 0.31$). Also, TFI-measured break-up time significantly correlated with the clinical measure of tear break-up time ($r = 0.73$).

Figure 8 shows a typical thickness trend of the lipid and the muco-aqueous layers of a real human eye diagnosed as a dry eye at its central spot as measured by the spectrometer. The horizontal axis presents the time in seconds, and the vertical axis shows the thickness values in nanometers. There are two vertical axes: one for the lipid's thickness with the range 30–70 nm and a second for the aqueous layer's thickness with the range 3500–5000 nm. The repeated measurements of the muco-aqueous layer thicknesses are presented by the blue dots, while the lipid layer thicknesses are presented by the red dots. The discontinuities of the dots represent the time frames where the eye image was decentered or defocused. The blinks events are presented in the image as one or more vertical green lines.

As can be seen, the thickness of the lipid layer varies within a limited range, while the muco-aqueous layer's thickness undergoes a fast decay during the interblink time. The measured muco-aqueous layer's thickness change rates in this example were 50–400 nm/s, which might be considered as fast evaporation processes or unstable layers. As clinical data is accumulated, we will examine the layers' dynamic process, which we believe to indicate tear film stability and DE status.

Referring to Fig. 5, the range of the lipid's thickness is better than 20 nm over a 6.5 mm diameter of the cornea's surface. We have found that such narrow distribution of values is distinctive for healthy eyes when they are measured about 1 s after the blink, while DE with lipid problems presents a much wider thickness range, in line with previous reports [13].

The TFI captures both the wideband spectral measurement and the full-field color images at a high rate of more than

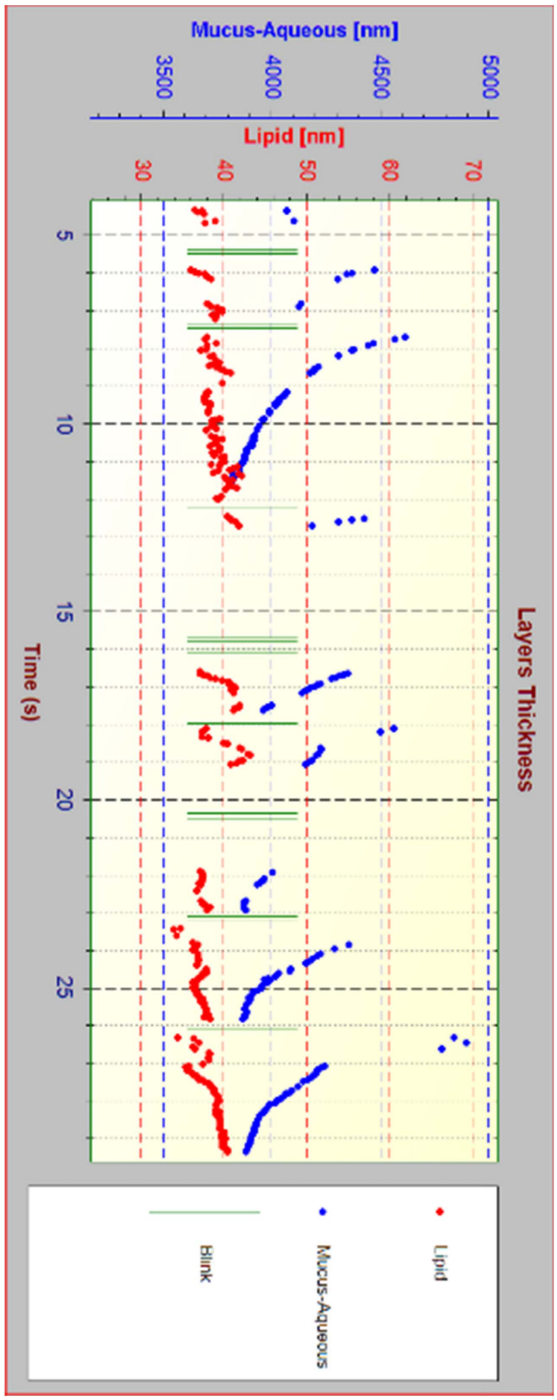

Fig. 8. Typical example for the lipid and muco-aqueous layers thickness values as measured by the TFI device versus time of measurement. Blue dots indicate the muco-aqueous layer, while red dots present the lipid layer (each with its corresponding axis) in the eye center; green lines indicate blinks.

10 times per second. This high rate of measurement supports a dynamic assessment of the tear film sublayers' dynamics, especially for the extreme case of severe evaporative DE tear films that present a high dynamic. Therefore, the homogeneity and the uniformity of the lipid and the muco-aqueous layers' thicknesses can be assessed for most patients.

6. CONCLUSION

The assessment of a tear film's muco-aqueous layer's thickness is challenging due to its low reflectance resulting in low signal-to-noise, which the TFI design overcomes based on a meticulous system design. This design enables the extraction of both the lipid and the muco-aqueous layers' thicknesses at a nanometer resolution and at a frequency high enough to track the layers' dynamics between blinks.

The model-based interpretation of the spectral measurements enables accurate reconstruction of the tear film inner layers as was validated both on a tear film mock-up and in a pilot clinical study. These measurements reveal the lipid and muco-aqueous layer's thickness dynamic behavior within the interblink interval, while the range of the measured thickness is in agreement with previous works [11,9].

The TFI-measured muco-aqueous dynamic thinning rate of 10–400 nm/s is in line with the average range of 17–167 nm/s (1–10 μm/min) reported before [8]. Interestingly, the TFI reports a thinning rate relaxation during the interblink interval (Fig. 8), a behavior that was not observed in previous works. The ability to observe the relaxation can be attributed to the higher accuracy combined with the more frequent measurements of the TFI.

The TFI overcomes the low signal-to-noise hurdles by simultaneously using different measurement modes and analysis techniques: spectrometry signal interpretation by regression convergence using a verified physical model and camera color analysis using concurrent calibrated imaging. By combining large-FOV color image acquisitions with fast spectrometric measurements, the TFI gives information about many attributes of the tear film in parallel, including the muco-aqueous layer thickness, the thickness change rate, the lipid layer thickness, and the tear break-up time. Other assistance techniques help to overcome specific system challenges such as a fixation target, fast autofocus response, and image analysis at a fast rate.

In addition to the precise muco-aqueous thickness evaluation, the TFI reports the lipid layer thickness at nanometer resolution and at high repetition rate. This accurate and frequent measurement enables us to explore the lipid layer interblink behavior at new levels of precision, while the overall range of lipid layer thickness as measured by the TFI is within the acceptable range [11]. In addition, the lipid layers' maps in a large FOV can be extracted by using the color images of the camera that are converted to accurate lipid thickness uniformity maps with repeated calibration by the spectrometric measurements. These images may be analyzed to reveal the tear break-up time.

The TFI measures its precise tear film measurements at the eye optical axis, where high-acuity vision take place. This eye section should be a high priority to resolve and ensure that central vision is untacked. We are still short of resolving the full muco-aqueous thickness map, although several ideas have been examined. The challenge of low reflectance aqueous layers coupled with highly dynamic tear films with off-axis imaging will be addressed in future work.

The system interferometric option that was described in Fig. 1 has an option to produce full muco-aqueous thickness mapping but at slower sampling rates. Our preliminary clinical results on human eye dynamics (Fig. 8) suggests that tear film

Fig. 9. Tear film imager prototype.

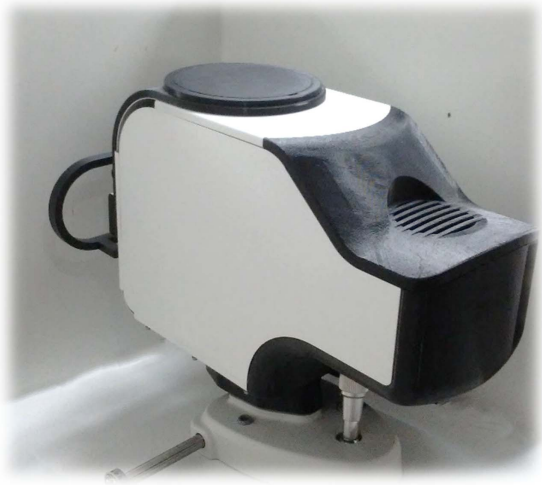

Fig. 10. Next-generation TFI.

thicknesses are fast changing, and therefore an interferometric solution may be deficient.

DE is an epidemic that suffers from lack of a good diagnostic. The TFI prototype (Fig. 9) described in this article can extract the tear film sublayers' structure and dynamics in a single device. Next-generation TFIs that have gone through engineering compactization could fit in everyday ophthalmology clinics (Fig. 10). The device can extract important attributes of the different parts of the tear film in a short, noninvasive test that might indicate on the state of the DE disease. This promising technology would benefit from further clinical validation with regard to different population groups, treatment efficiency, and more.

Funding. Israeli Innovation Authority (52259, 53285).

Acknowledgment. The TFI device was provided by AdOM Advanced Optical Technologies Ltd.

Disclosures. YA: AdOM, Advanced Optical Methods Ltd. (I,C); AH: CIPLA (C), AdOM (I,C), Oxymap (I), Shire (C).

REFERENCES

1. A. J. Bron, C. S. de Paiva, S. K. Chauhan, S. Bonini, E. E. Gabison, S. Jain, E. Knop, M. Markoulli, Y. Ogawa, V. Perez, Y. Uchino, N. Yokoi, D. Zoukhri, and D. A. Sullivan, "TFOS DEWS II pathophysiology report," Ocul. Surf. **15**, 438–510 (2017).
2. R. Potvin, S. Makari, and C. J. Rapuano, "Tear film osmolarity and dry eye disease: a review of the literature," Clin. Ophthalmol. **9**, 2039–2047 (2015).
3. S. C. Pflugfelder, F. Bian, and C. D. Paiva, "Matrix metalloproteinase-9 in the pathophysiology and diagnosis of dry eye syndrome," https://www.dovepress.com/matrix-metalloproteinase-9-in-the-pathophysiology-and-diagnosis-of-dry-peer-reviewed-article-MNM.
4. L. Tian, J. Qu, X. Zhang, and X. Sun, "Repeatability and reproducibility of noninvasive keratograph 5M measurements in patients with dry eye disease," J. Ophthalmol. **2016**, 8013621 (2016).
5. S. M. Lee, S. J. Chung, and H. Lew, "Evaluation of tear film lipid layer thickness measurements obtained using an ocular surface interferometer in nasolacrimal duct obstruction patients," Korean J. Ophthalmol. **32**, 445–450 (2018).
6. Y. Eom, J.-S. Lee, S.-Y. Kang, H. M. Kim, and J.-S. Song, "Correlation between quantitative measurements of tear film lipid layer thickness and meibomian gland loss in patients with obstructive meibomian gland dysfunction and normal controls," Am. J. Ophthalmol. **155**, 1104–1110 (2013).
7. R. Y. Kim, K. S. Na, Y. L. Park, and H. S. Kim, "Correlation analysis of tear film lipid layer thickness and ocular surface disease index," J. Korean Ophthalmol. Soc. **58**, 788–796 (2017).
8. P. E. King-Smith, B. A. Fink, and N. Fogt, "Three interferometric methods for measuring the thickness of layers of the tear film," Optom. Vis. Sci. **76**, 19–32 (1999).
9. P. E. King-Smith, B. A. Fink, N. Fogt, K. K. Nichols, R. M. Hill, and G. S. Wilson, "The thickness of the human precorneal tear film: evidence from reflection spectra," Invest. Ophthalmol. Vis. Sci. **41**, 3348–3359 (2000).
10. J. J. Nichols, G. L. Mitchell, and P. E. King-Smith, "Thinning rate of the precorneal and prelens tear films," Invest. Ophthalmol. Vis. Sci. **46**, 2353–2361 (2005).
11. P. E. King-Smith, E. A. Hinel, and J. J. Nichols, "Application of a novel interferometric method to investigate the relation between lipid layer thickness and tear film thinning," Invest. Ophthalmol. Vis. Sci. **51**, 2418–2423 (2010).
12. V. A. dos Santos, L. Schmetterer, M. Gröschl, G. Garhofer, D. Schmidl, M. Kucera, A. Unterhuber, J.-P. Hermand, and R. M. Werkmeister, "In vivo tear film thickness measurement and tear film dynamics visualization using spectral domain optical coherence tomography," Opt. Express **23**, 21043–21063 (2015).
13. H. Hwang, H.-J. Jeon, K. C. Yow, H. S. Hwang, and E. Chung, "Image-based quantitative analysis of tear film lipid layer thickness for meibomian gland evaluation," Biomed. Eng. Online **16**, 135 (2017).
14. Y. Arieli, Y. Cohen, S. Epstein, D. Arbel, and R. Gefen, "System and method for performing tear film structure measurement," U.S. patentUS9833139B1 (5December2017).
15. Y. Arieli, S. Epshtein, A. Harris, I. Yaacubov, and Y. Cohen, "Full field tomography using interference fringes casting of a non spatially-coherent extended spectrally modulated broadband light source," Opt. Commun. **407**, 426–431 (2018).
16. M. G. Moharam and T. K. Gaylord, "Rigorous coupled-wave analysis of planar-grating diffraction," J. Opt. Soc. Am. **71**, 811–818 (1981).
17. A. N. Bashkatov and E. A. Genina, "Water refractive index in dependence on temperature and wavelength: a simple approximation," Proc. SPIE **5068**, 393–396 (2003).
18. "Three dimension tomography of eye structures by white light imaging device-full text view-ClinicalTrials.gov," https://clinicaltrials.gov/ct2/show/NCT02424266.
19. F. Segev, N. Geffen, A. Galor, Y. Cohen, R. Gefen, A. Belkin, Y. Arieli, S. Epshtein, A. Oren, and A. Harris, "Dynamic assessment of the tear film muco-aqueous and lipid layers using a novel tear film imager (TFI)," Br. J. Ophthalmol., 313379 (2019).